Detectability and Configuration of Tropical Cyclone Eyes over the Western North Pacific in TRMM PR and IR Observations

YASU-MASA KODAMA AND TAKUYA YAMADA*

Department of Earth and Environmental Sciences, Hirosaki University, Hirosaki, Aomori, Japan

(Manuscript received 7 August 2003, in final form 26 January 2005)

ABSTRACT

Statistics for 138 cases from 61 tropical cyclones over the western North Pacific during the five years from 1998 to 2002 were used to determine the detectability and configuration of tropical cyclone (TC) eyes and to reveal relations with TC intensity and life stages in satellite-based infrared (IR) and precipitation radar (PR) observations from the Tropical Rainfall Measuring Mission (TRMM). Tropical cyclone eyes were detectable in PR data in 89% of cases and in IR data in 37% of cases. Maximum sustained wind speeds in TCs were much greater when the eye was detected in both IR and PR data than in cases when the eye was detected only in PR data or when no eye was detected in either PR or IR data. An eye was detectable in both IR and PR data in the developing stage of only 18% of TCs although an eye was present in the PR data in 90% of cases. An eye was detected in both IR and PR data in 51% of the TCs during the mature stage. During the decaying stage, an eye was detected in both IR and PR data in 31% of cases. Eye diameter determined from PR observations was larger during the later stages. Most TCs had an eye less than 82.5 km in diameter during the developing stage. Tropical cyclone eyes embedded within concentric eyewalls appeared more frequently in the mature and decaying stages; this is consistent with findings from previous studies. In most cases, eye diameter was smaller in IR observations than in PR observations because an upper cloud shield extending from the eyewall partially covered the eye. For several TCs with concentric eye walls, however, eye diameter was smaller in PR observations. A shallow inner eyewall in the PR data and a deep outer eyewall in both IR and PR data characterized these cases.

1. Introduction

In situ observations of well-developed tropical cyclones (TCs) over oceans are made difficult by the severe weather that is associated with such systems. Therefore, satellite remote sensing is a powerful tool for studying TCs. Many operational centers use cloud images of TCs taken from geostationary satellites to determine their position and to estimate sea level pressure (SLP) in the center. Furthermore, maximum sustained winds are estimated using the Dvorak technique (Dvorak 1975, 1984), which uses the location of the low-level circulation center and the configuration of the inner portion of TCs. However, satellite cloud images may fail to reveal the inner structure of TCs, especially the eye, if an upper-level cloud canopy obscures that part of the storm. Dvorak (1975, 1984) recognized this by creation of the central dense overcast pattern or the embedded eye pattern.

Radar observations can reveal the internal structures of TCs. Weatherford and Gray (1988) examined previous U.S. Air Force reconnaissance and showed statistics of eye size of TCs and their relation to minimum sea level pressure and outer-core wind speed. Airborne Doppler radars have recorded temporal variations in eyewalls and tangential winds in many TCs (Willoughby et al. 1982; Willoughby 1990; Black and Willoughby 1992). The eye of a TC and the accompanying wind maxima normally constrict as the TC intensifies. TCs with a single vigorous axisymmetric eyewall usually intensify rapidly. Tropical cyclone eye diameter can become very small (less than 10 km). An outer eyewall and a secondary wind maximum speed may form around the preexisting inner eyewall in an intense TC.

* Current affiliation: Disaster Prevention Research Group, National Science Institute for Earth Science and Disaster Prevention, Tsukuba, Ibaraki, Japan.

Corresponding author address: Yasu-Masa Kodama, Department of Earth and Environmental Sciences, Hirosaki University, Hirosaki, Aomori 036-8561, Japan.
E-mail: kodama@cc.hirosaki-u.ac.jp

The outer eyewall subsequently contracts, strangling the clear inner region and either halting intensification or weakening the TC. Willoughby et al. (1982) referred to this double-eye structure as a concentric ring. Mori et al. (1999) described the temporal evolution of convective activity in an initial-stage TC using shipborne radar and satellite-derived wind and cloud data. They showed that rapid development of the cyclonic circulation followed the appearance of a central dense overcast.

Statistical studies of TC eyes using precipitation radar (PR) were difficult prior to the launch of the Tropical Rainfall Measuring Mission (TRMM) in 1997. TRMM provided repeated spaceborne PR observations over open ocean for the first time. The PR instrument on the TRMM is a 13.8-GHz radar that can observe the 3D rainfall structures within a TC. Hereafter, these observations are called PR observations. The TRMM also carries a Visible and Infrared Scanner (VIRS) that provides IR cloud images in the atmospheric window, hereafter referred to as IR observations. TRMM IR images can be compared to IR observations from geostationary satellites, which have been used for the Dvorak technique.

This study examined the detectability, configuration, and diameter of TC eyes in PR observations and statistically related them to those in IR observations. The results from the statistical studies are used to discuss relationships with the intensity and life stage of TCs.

2. Data and analysis

The Japan Meteorological Agency (JMA) operates the Regional Specialized Meteorological Center (RSMC) Tokyo-Typhoon Center for the western North Pacific and the South China Sea. TCs over these regions are classified as "typhoons," "severe tropical storms," and "tropical storms" when maximum 10-min sustained wind speeds exceed 64 kt, are between 48 and 63 kt, and are between 34 and 47 kt, respectively. The Typhoon Committee for the western North Pacific Ocean and the South China Sea adopted these definitions. The Joint Typhoon Warning Center (JTWC), operated by the U.S. Navy and Air Force, uses different definitions. The JTWC classifies TCs as "supertyphoons," "typhoons," and "tropical storms" when maximum 1-min sustained wind speeds exceed 128 kt, are between 64 and 127 kt, and are between 34 and 63 kt, respectively. This study examines TCs that attained tropical storm intensity or higher in JMA analyses over the western North Pacific and the South China Sea between longitudes 100°E and 180°.

The study uses best track (BT) data from the RSMC Tokyo-Typhoon Center (http://www.jma.go.jp/JMA_HP/jma/jma-eng/jma-center/rsmc-hp-pub-eg/RSMC_HP.htm) and data from the U.S. JTWC (https://metoc.npmoc.navy.mil/jtwc/atcr/atcr_archive.html). The former is hereafter referred to as BT-JMA and the latter as BT-JTWC. Center positions and minimum SLP were obtained from BT-JMA on the RSMC Web site. Minimum SLP information was unavailable at the JTWC Web site. Differences in center positions between the two best track datasets were small (not shown). Maximum wind speeds were analyzed using data from both agencies because of differences in the method of presenting maximum wind speeds. BT-JMA uses maximum 10-min sustained wind speeds, and BT-JTWC uses maximum 1-min sustained winds. Geostationary Meteorological Satellite (GMS) IR and visible cloud images are utilized in both datasets, as the primary data source for the Dvorak technique. The maximum 1-min sustained wind speed (from BT-JTWC) was derived using the Dvorak technique T number; the maximum 10-min sustained wind speed (from BT-JMA) was derived using a statistical relationship between the Dvorak current intensity number (CI number) and the maximum 10-min wind speed. This statistical relationship was determined in an analysis of TCs from 1981 to 1986. During these years, maximum sustained 10-min wind speeds were very reliable because of U.S. Air Force reconnaissance missions that flew during the period (Koba et al. 1990).

Tropical cyclone wind speed maxima from the two best track datasets were compared to wind speed maxima derived by the Quick Scatterometer (QuikScat) satellite (available on the QuikScat Web site, http://www.ssmi.com/qscat/qscat_browse.html). QuikScat wind speed maxima are determined from near-surface wind fields observed by SeaWinds, a scatterometer on the QuikBird satellite launched in 1999. Rain-flagged wind speeds, which are unreliable because of raindrops, are eliminated from the analysis. This processing does not guarantee that wind speeds near the eyewall, where speeds are usually strongest, will agree with maximum wind speeds determined by QuikScat data. Wind speed observations from QuikScat are snapshots that represent mean values over a 25-km^2 area, and the best agreement between QuikScat wind speeds and adjacent buoy observations is obtained when the latter are temporally averaged for 10–60 min (N. Ebuchi 2003, personal communication). Maximum TC wind speeds in best track data were examined for temporal and horizontal variations of the wind field, while those from the QuikScat were searched for horizontal variations in the wind field snapshots. Therefore, a precise one-to-one correspondence cannot be examined.

Despite these shortcomings, however, maximum TC

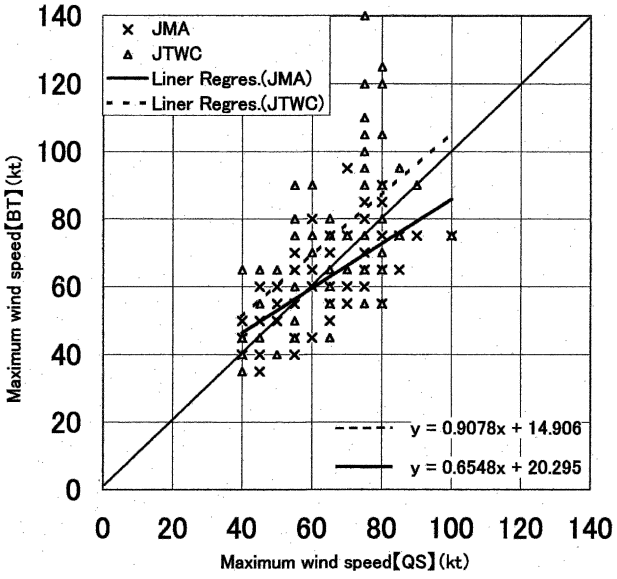

FIG. 1. Relationships between the 10-min sustained maximum wind from BT-JMA data, the 1-min sustained maximum wind from BT-JTWC data, and maximum wind speeds determined from QuikScat (QS).

wind speeds from the two best tracks are worth being compared to QuikScat wind speed maxima because the QuikScat is an independent data source obtained by an active remote sensor. Figure 1 shows the relationships between wind speed maxima from BT-JMA, BT-JTWC, and QuikScat. The time intervals for QuikScat data are approximately 12 h; only those cases in which the time difference between QuikScat data and each best track data was less than 4 h are plotted. The BT-JMA (BT-JTWC) wind speeds are weaker or equal to QuikScat winds, but the bias between them is not large (5–10 m s^{-1}). The different properties of the two best-track datasets become obvious for stronger winds. Wind speeds from BT-JTWC show large scatter when the BT-JMA wind speed exceeds 70 kt, and the bias between the BT-JTWC and BT-JMA increases. Part of this discrepancy may arise from the difference in the sustained wind sampling time of the two best track datasets. Therefore, results using maximum wind speeds will be shown for each best track dataset. Maximum wind speeds are obtained by temporally interpolating the 3- or 6-hourly wind speeds for each best track dataset.

The present study uses version 5 TRMM observation data products provided by the Goddard Space Flight Center (GSFC) of the National Aeronautics and Space Administration (NASA) and the Earth Observation Research and Application Center (EORC) of the Japan Aerospace Exploration Administration (JAXA). Precipitation radar observations are derived from attenuation-corrected precipitation intensity at 2 km ASL in the "2A25 product." Infrared observations arise from brightness temperature (TBB) analyses at 10.8 μm observed by VIRS channel 4 in the "1B01 product." Details of the algorithms used to compile these data products can be found in NASA GSFC (2002a,b). Horizontal resolution differs for the two products: it is 4.3 km for PR and 2 km for IR. Therefore, data were resampled into 0.05° (latitude) × 0.05° (longitude) coordinates for comparisons between the two observation types. A gridpoint value in the latitude–longitude coordinates was assigned the value at the closest point in the data coordinates along the TRMM orbit. Interpolation was not applied. The horizontal resolution of the latitude–longitude coordinates is ~5 km, so eyes with a diameter of less than 10 km may not be detected, as reported by Black and Willoughby (1992). From 7 to 24 August 2001, the TRMM orbit altitude was increased from 350 to 402 km to reduce atmospheric resistance and thereby lengthen the observation life of TRMM. This change degraded the horizontal resolution of each sensor by 15%. The horizontal resolution of the 2A25 and 1B01 products is smaller than the latitude–longitude grid intervals (~5 km) even after the orbit alteration, so the orbital change had little influence on the present results.

The PR observation swath is fairly narrow (~215 km), so the repeat time of PR observations in the Tropics is several days. Therefore, although PR observations cannot describe the temporal evolution of individual TCs, statistical features of TCs can be discussed when many PR observations for many different TCs are analyzed. The local time of TRMM observations is not biased because the TRMM orbit is not sun-synchronous. Therefore, diurnal variations in TCs (e.g., Muramatsu 1983) do not contaminate the statistics. Despite the low frequency of observations, during the five years from 1998 to 2002 there were 138 cases from 61 TCs in which the TC center was in the PR observation swath. TCs with centers over land or close to land were excluded to prevent "land effects" from contaminating the statistics. The Tropical Cyclone Database (http://www.eorc.jaxa.jp/TRMM/typhoon/index_e.htm) maintained by JAXA-EORC facilitated the search for cases.

The configuration of the central portion of TCs as represented in IR and PR observations was compared. An eyewall around the center of a TC in PR data was defined as a curved band with precipitation intensity exceeding 0.5 mm h^{-1} at 2 km ASL. Three configurations of the inner precipitation area of TCs in PR observations were categorized, and another, separate, category is also defined:

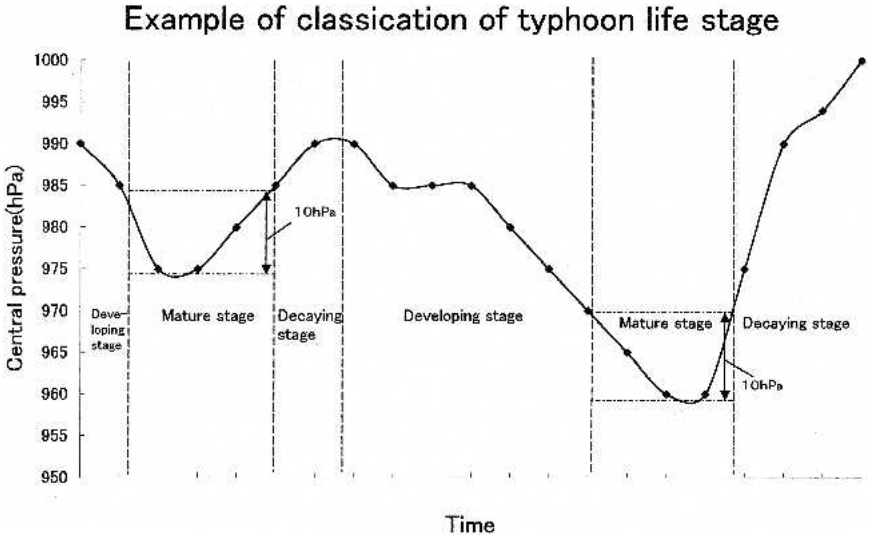

FIG. 2. The model to explain TC life stage classification used in this study.

- Ring: A continuous or intermittent eyewall surrounding more than 270° of the center, except for gaps of less than 30°. This category is a completed eye pattern.
- Arc: A continuous or intermittent eyewall surrounding more than 180° of the typhoon center, except for gaps. No constraints exist for the gaps except to be less than 180° in total. This category is an incomplete eye pattern.
- None: Other than the ring and the arc. This category is the no-eye pattern. Sometimes only a straight precipitation band appeared. Ring and arc (none) cases were considered as detectable (undetectable) typhoon eyes in this study.
- Concentric: A concentric ring (Willoughby et al. 1982) exists when one or more outer eye walls surrounds the inner precipitation core for more than 180° with or without interruptions. Concentric was defined independently of the other three categories, which were defined only for the inner precipitation core. Concentric may exist when no eye was detected in the inner precipitation core.

Infrared observations of TC cloud configurations were categorized into "eye pattern," "curved band," "shear pattern," and "embedded eye pattern," referred to as EYE, CVB, SHR, and EMB, respectively. Such classification follows the Dvorak enhanced IR (EIR) method (Dvorak 1984). Cloud configuration was manually classified by the first author using TBB fields from 10.8-μm data, which were displayed using the grayscale for the EIR method. Cloud pattern classification is not perfect but is reliable; an expert on typhoon analysis using the Dvorak technique (S. Akashi 2004, personal communication) lent advice.

Eye position was defined as the geometric center of the surrounding eyewall. Eye diameter was determined as an average of the longer and shorter inside diameters of the eye (or of the clear inner core, when concentric eyewalls existed) in PR and IR observations.

Figure 2 shows definitions of three life stages used in the study of the relationship between detectability and configuration of eyes and TC life cycles. Short-period (less than one day) variations in the center SLP of a TC were ignored, and one or several minima in the temporal variation of the SLP were determined. The mature stage was defined as occurring when the SLP was within 10 hPa of each minima. Periods other than the mature stage were classified as developing, when the SLP was decreasing, and decaying, when the SLP was increasing. Table 1 lists all information for the collected TCs in this study. The cases are spread over a wide latitude range and include TCs at various life stages.

3. Typhoon eyes in PR and IR observations

Several examples of TC images from PR and IR observations show different degrees of detectability for typhoon eyes. Figures 3a and 3b show Typhoon Bart, a case where a small, significant eye was detected in both types of observations. Once mature, this intense typhoon had maximum sustained wind speeds of 85 kt according to BT-JMA (140 kt according to BT-JWTC). A concentric outer eyewall (Willoughby et al. 1982) was present. The two observation datasets show the same eye position. However, significant discrepancies exist between the fields of precipitation intensity and TBB, which corresponds to cloud-top temperature. Precipitation radar observations show a significant eye-

TABLE 1. Information for all cases analyzed, including date and time (UTC) of observations, latitude and longitude of TC center position, number and name of TC, maximum 10-min sustained wind speed from BT-JMA data, maximum 1-min wind speed from BT-JTWC data, maximum wind speed from QuikScat (QS), TC eye diameter in IR and PR observations, whether the eye was detected by each sensor, TC cloud configuration in IR observation as categorized by the Dvorak technique (EYE: eye detectable; SHR: shear pattern; CVB: curved band; and EMB: embedded eye pattern), configuration of typhoon eyes in PR observations (Co: Concentric), life stage of typhoons (DV: developing stage; MT: mature stage; and DC: decaying stage), and the orbit number of the TRMM observation.

	Date	Time (UTC)	Position Lat	Position Lon	No.	Name	Wind speed (kt) (JMA)	Wind speed (kt) (JTWC)	Wind speed (kt) (QS)	Diameter (km) (IR)	Diameter (km) (PR)	Configuration (IR)	Configuration (PR)	Stage	Orbit No. (TRMM)
1	25 Aug 1998	2018	25	135	9804	Rex	50	60	—	—	60	CVB	Ring	DV	4273
2	29 Aug 1998	1843	29	141	9804	Rex	75	95	—	30	110	EYE	Ring	MT	4335
3	30 Aug 1998	2221	31	143	9804	Rex	70	90	—	30	75	EYE	Arc	MT	4353
4	3 Sep 1998	1910	32	155	9804	Rex	65	65	—	—	45	CVB	Ring	DC	4414
5	4 Sep 1998	1445	32	158	9804	Rex	60	65	—	—	30	CVB	Arc	DC	4427
6	5 Sep 1998	1509	34	158	9804	Rex	55	55	—	—	—	CVB	None	DC	4443
7	13 Sep 1998	1642	22	140	9805	Stella	35	45	—	—	300	CVB	Arc	DV	4570
8	15 Sep 1998	1415	32	136	9805	Stella	60	65	—	—	—	EMB	None	MT	4600
9	18 Sep 1998	0859	30	132	9806	Todd	55	65	—	—	230	CVB	Arc	DC	4644
10	18 Sep 1998	1349	30	128	9806	Todd	50	65	—	—	75	EMB	Arc	DC	4647
11	21 Sep 1998	0659	26	132	9807	Vicki	65	65	—	—	75	EMB	Ring	MT	4690
12	15 Oct 1998	0206	19	121	9810	Zeb	90	85	—	—	180	CVB	Ring	DC	5065
13	17 Oct 1998	0120	13	130	9811	Babs	35	45	—	—	30	SHR	Arc	DV	5096
14	18 Oct 1998	1448	12	130	9811	Babs	40	45	—	—	30	EMB	Ring	DV	5127
15	19 Oct 1998	0032	10	130	9811	Babs	55	65	—	—	15	EMB	Ring	DV	5158
16	23 Oct 1998	1333	17	119	9811	Babs	65	80	—	—	20	CVB	Ring	MT	5235
17	25 Oct 1998	2049	21	117	9811	Babs	70	70	—	—	120	CVB	Ring	MT	5246
18	23 Apl 1999	2319	15	128	9901	Kate	40	50	—	—	30	CVB	Arc	DV	8075
19	26 Apl 1999	1314	22	136	9901	Kate	50	65	—	—	75	EMB	Arc	MT	8116
20	29 Apl 1999	1245	18	114	9902	Leo	50	55	—	—	30	EMB	Arc	DV	8163
21	29 Apl 1999	2050	18	114	9902	Leo	60	65	—	—	45	CVB	Ring	MT	8168
22	1 May 1999	1157	21	115	9902	Leo	50	70	—	—	—	CVB	None	DC	8194
23	3 Jun 1999	1725	17	128	9903	Maggie	60	80	—	—	15	EMB	Ring, Co	DV	8718
24	6 Jun 1999	0040	22	120	9903	Maggie	55	90	—	—	—	CVB	None, Co	DC	8754
25	26 Jul 1999	1624	32	128	9905	Neil	50	40	—	—	40	EMB	Ring	MT	9553
26	26 Jul 1999	1937	32	128	9905	Neil	50	40	50	—	45	CVB	Ring	MT	9555
27	30 Jul 1999	1939	21	132	9907	Olga	50	55	45	—	15	CVB	Ring	DV	9618
28	31 Jul 1999	1157	23	130	9907	Olga	50	65	50	—	40	CVB	Ring	MT	9629
29	5 Aug 1999	1536	27	132	9908	Paul	45	35	40	—	45	CVB	Arc	DV	9710
30	21 Aug 1999	0425	31	168	9912	Tanya	50	65	40	45	50	EYE	Ring	MT	9955
31	25 Aug 1999	2217	27	145	9913	Virgil	50	65	40	—	45	SHR	Ring	MT	10 030
32	15 Sep 1999	1252	22	115	9915	York	55	65	70	60	85	EYE	Ring	MT	10 355
33	18 Sep 1999	1230	31	123	9917	Ann	40	45	—	—	—	EMB	None	DC	10 402
34	20 Sept 1999	1005	24	126	9918	Bart	55	80	55	15	15	EYE	Ring	DV	10 432
35	20 Sep 1999	1632	24	126	9918	Bart	70	100	—	20	30	EYE	Ring	DV	10 436
36	22 Sep 1999	0917	26	127	9918	Bart	85	140	75	15	10	EYE	Ring, Co	MT	10 463
37	3 Oct 1999	1030	28	128	9920	Dan	35	45	45	—	60	EMB	Ring	DV	10 637
38	7 Oct 1999	0850	20	118	9920	Dan	75	90	90	30	90	EYE	Ring	MT	10 699
39	8 Oct 1999	0110	22	118	9920	Dan	75	90	—	60	70	EYE	Ring	DC	10 710
40	3 Jul 2000	1226	17	132	0003	Krogi	50	55	—	—	50	CVB	Arc	DV	14 959
41	5 Jul 2000	0333	20	132	0003	Krogi	85	115	—	40	75	EYE	Arc	MT	14 985
42	7 Jul 2000	1045	20	119	0004	Kai-Tak	75	75	70	10	120	EYE	Arc	MT	15 021
43	26 Jul 2000	1702	27	130	0006	Bolaven	45	45	—	—	—	SHR	None	MT	15 344
44	2 Aug 2000	1151	23	147	0008	Jelawat	75	115	—	10	15	EYE	Ring	DV	15 432
45	5 Aug 2000	1751	26	133	0008	Jelawat	80	90	60	70	75	EYE	Ring	DC	15 483
46	7 Aug 2000	1701	27	128	0008	Jelawat	75	85	—	150	105	EYE	Ring, Co	DC	15 514
47	8 Aug 2000	1058	28	127	0008	Jelawat	75	80	65	150	105	EYE	Ring, Co	DC	15 526
48	13 Aug 2000	0811	32	140	0009	Ewiniar	50	45	—	—	25	CVB	Arc	MT	15 603
49	14 Aug 2000	0837	34	145	0009	Ewiniar	50	45	65	—	45	CVB	Ring	MT	15 619
50	14 Aug 2000	1013	34	146	0009	Ewiniar	50	45	65	—	70	CVB	Ring	MT	15 620
51	15 Aug 2000	0901	35	149	0009	Ewiniar	60	75	60	45	60	EYE	Ring	MT	15 635
52	27 Aug 2000	0721	22	130	0012	Prapiroon	40	35	—	—	75	SHR	Arc	DV	15 823

TABLE 1. (*Continued*)

	Date	Time (UTC)	Position Lat	Position Lon	No.	Name	Wind speed (kt) (JMA)	Wind speed (kt) (JTWC)	Wind speed (kt) (QS)	Diameter (km) (IR)	Diameter (km) (PR)	Configuration (IR)	Configuration (PR)	Stage	Orbit No. (TRMM)
53	30 Aug 2000	0517	29	123	0012	Prapiroon	65	75	—	105	120	EYE	Ring	MT	15 869
54	31 Aug 2000	0051	33	124	0012	Prapiroon	70	70	—	120	120	EYE	Arc	MT	15 882
55	31 Aug 2000	0227	34	124	0012	Prapiroon	70	70	—	—	120	CVB	Arc	MT	15 883
56	4 Sep 2000	0233	16	152	0014	Saomai	60	65	—	—	30	EMB	Ring	MT	15 946
57	7 Sep 2000	1824	25	131	0015	Bopha	45	45	40	—	40	EMB	Ring	MT	16 004
58	8 Sep 2000	0055	18	142	0014	Saomai	55	65	—	—	25	EMB	Arc	DV	16 008
59	11 Sep 2000	1647	26	130	0014	Saomai	85	110	—	45	45	EYE	Ring	DC	16 066
60	12 Sep 2000	2202	‘27	127	0014	Saomai	75	90	80	30	120	EYE	Arc	DC	16 085
61	14 Sep 2000	2112	28	125	0014	Saomai	65	75	85	15	25	EYE	Ring	DC	16 116
62	15 Sep 2000	1336	24	141	0017	Sonamu	45	45	—	—	40	CVB	Arc	MT	16 127
63	15 Sep 2000	1647	33	128	0014	Saomai	60	65	—	—	45	CVB	Ring	DC	16 129
64	15 Sep 2000	1824	34	128	0014	Saomai	60	65	—	—	60	CVB	Arc	DC	16 130
65	15 Sep 2000	2004	25	141	0017	Sonamu	45	60	55	—	10	EMB	Ring, Co	DV	16 131
66	16 Sep 2000	1851	29	141	0017	Sonamu	45	70	60	—	55	EMB	Arc	MT	16 146
67	4 Nov 2000	2059	17	117	0021	Bebinca	55	55	—	—	30	EMB	Arc	MT	16 920
68	14 May 2001	1003	27	129	0101	Cimaron	35	50	—	—	45	CVB	Arc	MT	19 925
69	5 Jul 2001	0655	21	118	0104	Utor	60	65	70	—	290	CVB	Ring	MT	20 743
70	24 Jul 2001	0455	20	118	0107	Yutu	50	70	—	60	75	EYE	Ring	MT	21 041
71	25 Jul 2001	2007	29	141	0106	Kong-Rey	65	80	80	15	40	EYE	Ring	MT	21 067
72	26 Jul 2001	0057	29	141	0106	Kong-Rey	70	80	—	15	45	EYE	Ring	MT	21 070
73	26 Jul 2001	2346	31	144	0106	Kong-Rey	70	85	—	15	45	EYE	Ring	MT	21 085
74	27 Jul 2001	1921	33	147	0106	Kong-Rey	65	70	80	—	75	SHR	Arc	MT	21 098
75	27 Jul 2001	2234	33	148	0106	Kong-Rey	65	65	80	30	75	EYE	Arc	DC	21 100
76	5 Aug 2001	1944	26	144	0109	Man-Yi	80	105	75	15	40	EYE	Ring, Co	MT	21 240
77	27 Aug 2001	0958	18	142	0112	Wutip	40	45	45	—	60	CVB	Arc	DV	21 578
78	28 Aug 2001	0056	25	162	0113	Sepat	40	45	—	—	30	CVB	Arc	MT	21 588
79	28 Aug 2001	0903	21	143	0112	Wutip	65	85	—	15	30	EYE	Ring	DV	21 593
80	29 Aug 2001	0807	24	146	0112	Wutip	85	125	80	15	20	EYE	Ring	MT	21 608
81	30 Aug 2001	0711	26	147	0112	Wutip	85	120	80	30	55	EYE	Ring	MT	21 623
82	2 Sep 2001	0110	34	154	0112	Wutip	50	55	—	—	—	SHR	None	DC	21 666
83	2 Sep 2001	0248	35	154	0112	Wutip	50	55	—	—	90	SHR	Arc	DC	21 667
84	4 Sep 2001	2044	19	150	0115	Danas	65	70	60	—	10	EMB	Ring	DV	21 710
85	7 Sep 2001	2112	28	143	0115	Danas	80	100	75	15	30	EYE	Ring	MT	21 757
86	8 Sep 2001	0340	27	128	0116	Nari	60	65	—	—	10	EMB	Ring	MT	21 761
87	8 Sep 2001	2150	28	126	0116	Nari	60	65	50	—	45	CVB	Ring, Co	MT	21 773
88	11 Sep 2001	0231	26	126	0116	Nari	65	90	—	30	15	EYE	Ring	MT	21 807
89	15 Sep 2001	0026	26	124	0116	Nari	60	65	65	110	75	EYE	Ring, Co	DV	21 868
90	19 Sep 2001	1951	32	139	0117	Vipa	60	65	45	15	30	EYE	Arc	MT	21 943
91	20 Sep 2001	1719	36	143	0117	Vipa	65	75	55	15	20	EYE	Arc	MT	21 957
92	20 Sep 2001	2038	18	155	0118	Francisco	40	50	55	—	—	CVB	None	DV	21 959
93	22 Sep 2001	1344	20	124	0119	Lekima	35	35	—	—	45	SHR	Ring	DV	21 986
94	24 Sep 2001	1652	32	146	0118	Francisco	65	75	85	—	150	CVB	Arc	DC	22 019
95	25 Sep 2001	1235	21	121	0119	Lekima	65	90	—	—	15	CVB	Arc, Co	MT	22 032
96	21 Oct 2001	1951	13	156	0122	Podul	65	75	75	—	45	EMB	Arc	DV	22 442
97	24 Oct 2001	0351	17	157	0122	Podul	85	140	—	45	20	EYE	Ring, Co	DV	22 478
98	8 Nov 2001	2240	13	119	0123	Lingling	55	60	65	—	35	EMB	Arc	DV	22 724
99	17 Dec 2001	0124	6	162	0125	Faxai	35	35	—	—	60	CVB	Arc	DV	23 318
100	18 Dec 2001	1339	5	161	0125	Faxai	40	55	—	—	30	EMB	Ring	DV	23 342
101	20 Dec 2001	2317	9	158	0125	Faxai	65	75	—	—	15	CVB	Ring	DV	23 379
102	2 Mar 2002	1214	8	141	0202	Mitag	70	90	55	—	45	EMB	Ring	DV	24 494
103	6 Mar 2002	1006	16	130	0202	Mitag	85	120	75	45	55	EYE	Ring	MT	24 555
104	7 Mar 2002	0059	17	132	0202	Mitag	95	75	70	—	15	CVB	Arc	DC	24 565
105	7 Mar 2002	0911	18	133	0202	Mitag	65	70	—	—	—	CVB	None	DC	24 570
106	16 May 2002	2129	13	141	0203	Hagibis	45	45	—	—	—	EMB	None	DV	25 669
107	10 Jun 2002	0801	28	127	0204	Noguri	60	65	45	—	30	EMB	Arc	MT	26 050
108	30 Jun 2002	2228	6	154	0206	Chataan	50	50	—	—	30	EMB	Arc	MT	26 371
109	1 Jul 2002	1140	8	153	0206	Chataan	50	50	—	—	—	CVB	None	MT	26 380

TABLE 1. (*Continued*)

	Date	Time (UTC)	Position Lat	Position Lon	No.	Name	Wind speed (kt) (JMA)	Wind speed (kt) (JTWC)	Wind speed (kt) (QS)	Diameter (km) (IR)	Diameter (km) (PR)	Configuration (IR)	Configuration (PR)	Stage	Orbit No. (TRMM)
110	3 Jul 2002	1438	25	123	0205	Rammasun	85	110	—	60	55	EYE	Ring, Co	MT	26 413
111	4 Jul 2002	2021	14	145	0206	Chataan	70	90	75	15	45	EYE	Ring	DV	26 432
112	8 Jul 2002	0827	9	152	0207	Halong	40	40	40	—	15	EMB	Arc	DV	26 487
113	8 Jul 2002	1818	10	152	0207	Halong	45	45	55	—	—	CVB	None	DV	26 493
114	10 Jul 2002	0812	11	144	0207	Halong	60	95	75	—	30	CVB	Ring	DV	26 518
115	11 Jul 2002	1031	26	127	0208	Nakri	85	40	—	—	—	EMB	None	MT	26 535
116	13 Jul 2002	0840	21	131	0207	Halong	85	135	—	45	40	EYE	Ring, Co	MT	26 565
117	15 Jul 2002	1321	31	133	0207	Halong	60	55	75	—	—	CVB	None	DC	26 599
118	17 Jul 2002	0327	15	167	0209	Fengshen	90	125	80	15	5	EYE	Ring	MT	26 624
119	21 Jul 2002	0257	20	155	0209	Fengshen	95	140	—	20	20	EYE	Ring, Co	MT	26 686
120	21 Jul 2002	0432	23	138	0210	Kalmaegi	35	25	—	—	45	EMB	Arc	DC	26 687
121	23 Jul 2002	0915	27	145	0209	Fengshen	80	100	—	15	20	EYE	Arc	DC	26 721
122	23 Jul 2002	1050	22	131	0211	Fung-Wong	70	65	75	5	10	EYE	Ring	MT	26 722
123	25 Jul 2002	0226	21	134	0211	Fung-Wong	60	60	—	—	75	CVB	Arc	MT	26 748
124	25 Jul 2002	0405	30	132	0209	Fengshen	90	125	—	—	230	CVB	Arc	DC	26 749
125	17 Aug 2002	1538	29	138	0213	Phanfong	80	110	—	55	75	EYE	Ring	MT	27 115
126	19 Aug 2002	1526	34	142	0213	Phanfong	65	60	—	—	30	EMB	Arc	DC	27 146
127	24 Aug 2002	1724	20	154	0215	Rusa	55	70	—	—	45	EMB	Arc	DV	27 225
128	27 Aug 2002	0937	24	140	0215	Rusa	75	95	85	15	10	EYE	Ring, Co	MT	27 267
129	27 Aug 2002	1609	25	138	0215	Rusa	75	95	—	10	30	EYE	Arc, Co	MT	27 271
130	30 Aug 2002	0654	22	153	0216	Sinlaku	55	55	65	45	60	EYE	Ring	DV	27 312
131	30 Aug 2002	1005	30	129	0215	Rusa	75	75	100	75	150	EYE	Ring, Co	MT	27 314
132	1 Sep 2002	0639	24	145	0216	Sinlaku	70	110	75	30	30	EYE	Ring	MT	27 343
133	2 Sep 2002	0413	23	175	0217	Ele	90	105	80	30	15	EYE	Ring	MT	27 357
134	29 Oct 2002	0525	31	166	0223	Maysak	55	55	80	—	120	SHR	Arc	MT	28 246
135	5 Nov 2002	0350	21	164	0224	Huko	70	75	65	—	—	EMB	None	MT	28 354
136	22 Nov 2002	1238	17	138	0225	Haishen	55	65	50	—	—	CVB	None	DV	28 625
137	4 Dec 2002	1443	8	159	0226	Pongsona	45	50	—	—	60	CVB	Arc	DV	28 813
138	10 Dec 2002	1043	23	148	0226	Pongsona	80	80	—	—	30	CVB	Ring, Co	MT	28 904

wall, but IR observations show TBB minima not over the inner core but over the outer eyewalls to the west of the eye.

Figures 3c and 3d show Typhoon Ewiniar, a case in which an eye was detected in both observations, with some differences in eye configuration. This typhoon was in the decaying stage and had a maximum wind speed of 60 kt according to BT-JMA (75 kt according to BT-JWTC). The eyewall was vague in the southwestern quadrant in PR data, but the center of the typhoon was detected from the curvature. Low TBB clouds were east of the center in the IR data. These cold clouds were canopies that extended from active eyewall convection in the eastern quadrant of the storm. Part of the cloud canopy extended into the storm center and distorted the circular shape of the eye in IR data. Precipitation radar observations showed a nearly circular eyewall. Further discrepancies between PR and IR observations were found. For example, low TBB (cold) eyewall clouds in the northwestern quadrant were not accompanied by strong rainfall.

Figures 3e and 3f show Typhoon Babs, a case in which no eye was detected in IR data despite the significant eye detected in PR data. This typhoon was in the developing stage, and the maximum wind speed was 40 kt according to both BT-JMA and BT-JWTC. The discrepancy between the two observations results from a cloud canopy over the eye. The canopy covered the area from 9.2° to 11°N and 128.8° to 130°E in the IR data, corresponding to case EMB in the Dvorak technique. Figures 3g and 3h show Typhoon Maggie, a case in which no eye was detected in IR or PR data. This typhoon was in the decaying stage, with maximum wind speeds of 55 kt according to BT-JMA data (90 kt according to BT-JWTC). A large ring of convection surrounds a small, circular area of convection at the center of the TC. This structure is classified as "concentric" in this study. Precipitation radar data contained no eye; however, a trace of eyewalls was observed in echo-top height determined by PR data and 85-GHz TBB fields observed by the TRMM Microwave Imager (TMI; not shown). An inner eyewall may persist at upper levels, although an eye, that is, inner precipitation free region, was not detected at 2 km ASL. A possible reason is that

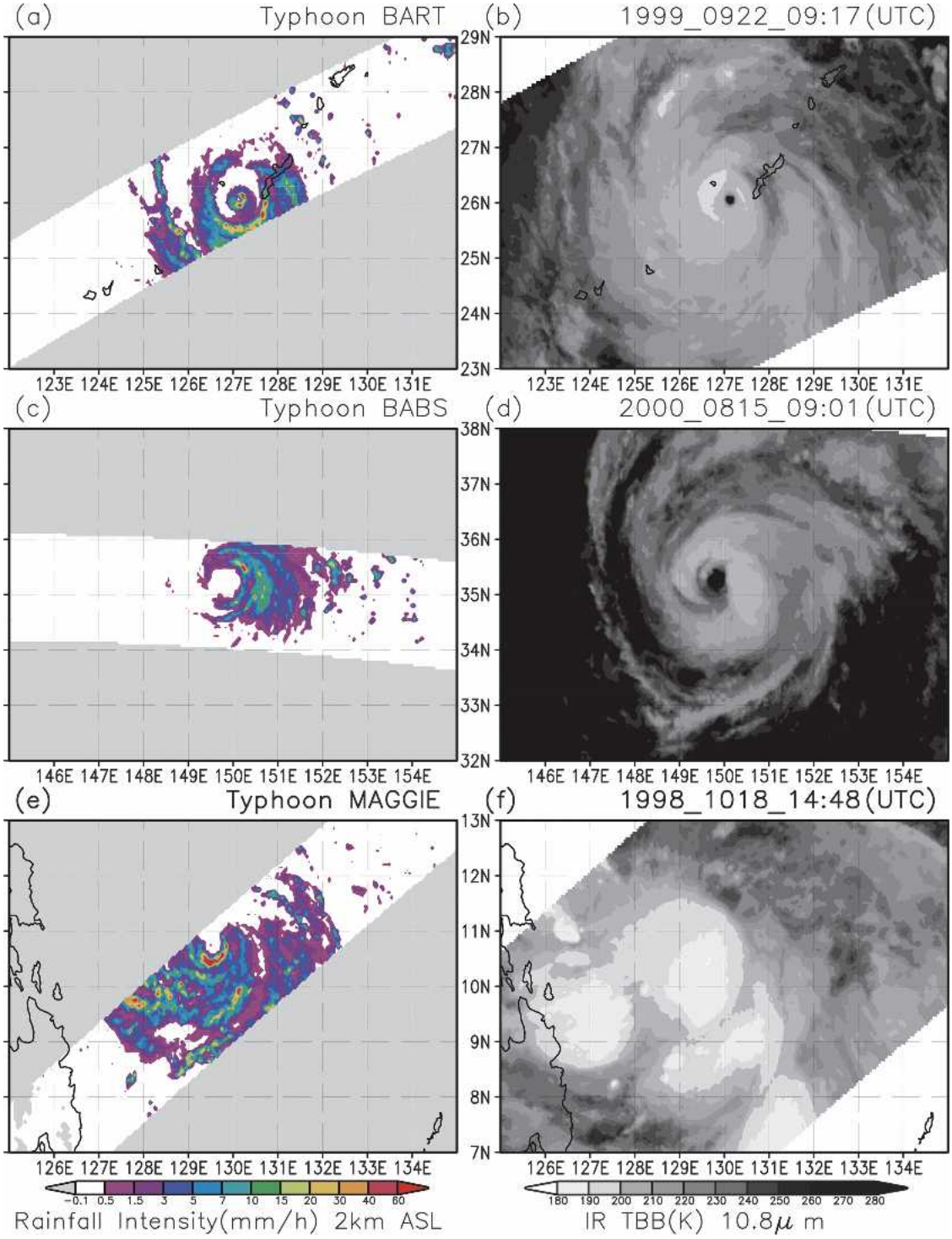

FIG. 3. (left) Rainfall intensity at 2 km ASL (observed by TRMM-PR) and (right) TBB (observed at 10.8 μm by TRMM-VIRS). Regions outside the PR swath are shaded gray in the left panels: (a), (b) the mature stage of Typhoon Bart (9918) at 9 h 17 m (UTC), 22 Sep 1999; (c), (d) the decaying stage of Typhoon Ewiniar (0009) at 9 h 01 m (UTC), 15 Aug 2000; (e), (f) the developing stage of Typhoon Babs (9811) at 14 h 48 m (UTC), 18 Oct 1998; (g), (h) the decaying stage of Typhoon Maggie (9903) at 0 h 40 m (UTC), 6 Jun 1999; (i), (j) the decaying stage of Typhoon Jelawat (0008) at 10 h 58 m (UTC), 8 Aug 2000.

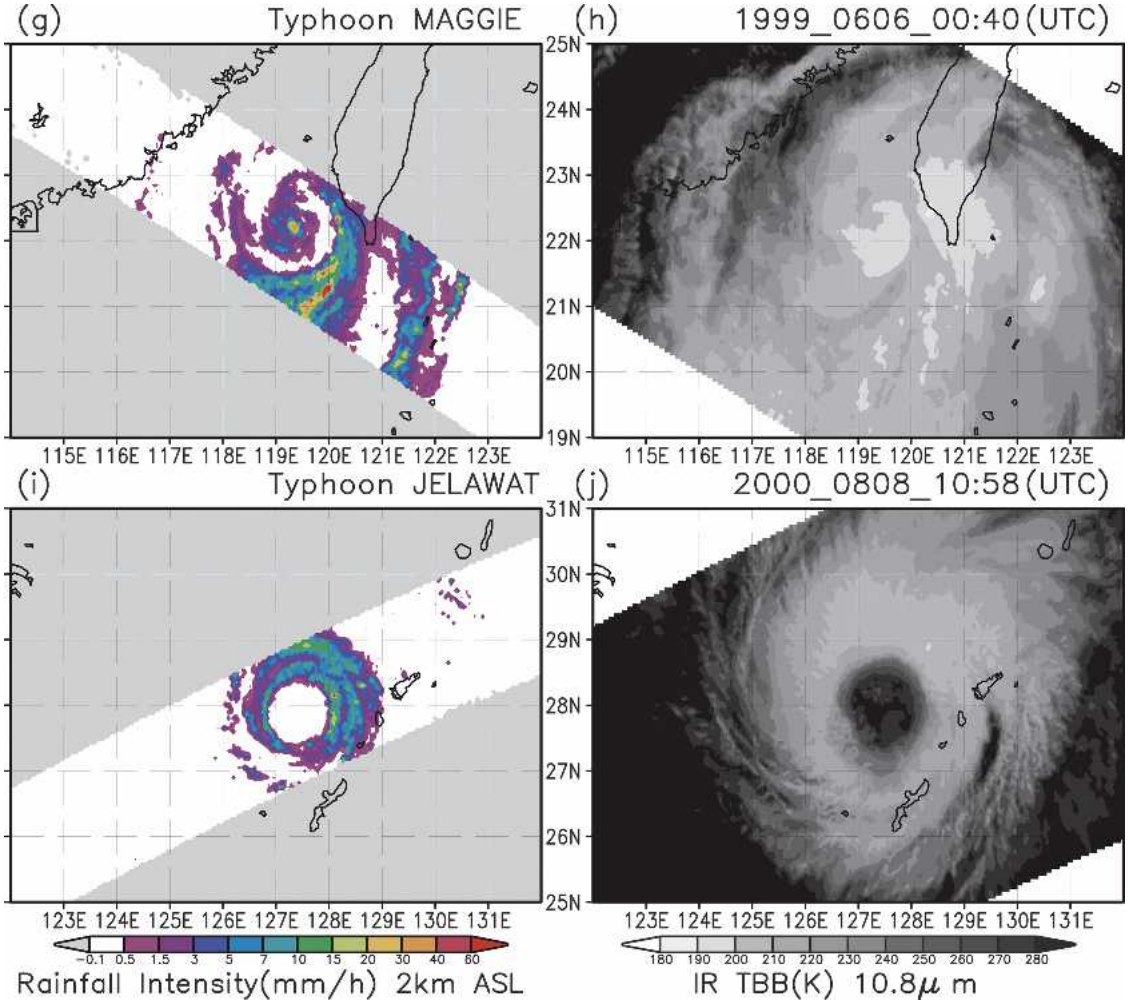

FIG. 3. (*Continued*)

eye size at low level was too small to be resolved by the PR data.

Figures 3i and 3j show Typhoon Jelawat, a case in which a large eye was detected in both IR and PR observations; the eye was larger in the IR data. This typhoon was in the decaying stage, with a maximum wind speed of 75 kt according to BT-JMA (85 kt according to BT-JTWC). Eye diameter was 105 km in PR data and 150 km in IR data. Precipitation radar observations show that Jelawat had concentric eyewalls. A significant cloud ring marked the outer eyewall in the IR data, which also showed low-level clouds inside the eye surrounded by a significant upper cloud ring. This suggests that the shallow clouds maintained the inner eyewall present in the PR data. Indeed, 17-dBZ radar echoes reached to ~3 km in the inner eyewall, and to more than 12 km in the outer eyewall (not shown). Lander (1999) described Typhoon Winnie, which had an eye with a diameter of 370 km in satellite cloud images. Observations from ground-based radar [Next-Generation Weather Radar (NEXRAD), Weather Surveillance Radar-1988 Doppler (WSR 88D)] also showed concentric eyewalls, and only the outer eyewall showed a complete ring of deep convection. Willoughby et al. (1982) remarked that development of the outer eyewall weakens and eventually destroys the inner eyewall.

4. Statistical relationship of eye detectability to the intensity and life stage of TCs

The last section showed that typhoon eyes are characterized differently in IR and PR observations. Consequently, eye detectability was analyzed statistically by counting the number of cases classified into four categories according to the detectability of the eyes in IR and PR observations (Table 2). Eyes were detected in IR data in 51 out of 138 (37%) cases. Eyes detected in

TABLE 2. The number of cases categorized by eye configuration in PR and IR observations. The configuration in PR is classified as ring, arc, and none.

	Eye in IR	No eye in IR	Total
Ring in PR	40 (29%)	33 (24%)	73 (53%)
Arc in PR	11 (8%)	38 (27%)	49 (36%)
None in PR	0 (0%)	16 (12%)	16 (12%)
Total	51 (37%)	87 (63%)	138 (100%)

PR data were categorized as "ring" or "arc" ("ring" only) for 122 (73) cases, or 89% (53%) of the total. No eyes were detected in either PR or IR data for only 16 cases, or 12% of the total. In no cases were eyes detected in IR data but not PR data. The results show that PR data reveal complete or incomplete eyes in most TCs. Infrared observations fail to detect eyes in half of the cases in which eyes were detected in PR.

The relationship between eye detectability in the two remote observational datasets and the maximum 10-min sustained wind speed from BT-JMA (Fig. 4) was analyzed. Mean wind speeds were highest (72.5 kt) when eyes were detected in both IR and PR data. Wind speeds were much lower for cases when eyes were detected only in PR data or when eyes were not detected in either PR or IR data. Eye detectability in IR data was more difficult for weaker TCs. A notable exception was Typhoon Nakri at 1031 UTC on 11 July 2002. No eye was detected in either PR or IR data despite winds that, according to the BT-JMA, exceeded 85 kt. The JTWC for this case showed a much smaller wind speed maximum (40 kt). The JTWC wind speed arises from faithful application of the Dvorak technique to the IR image, so the reason for the discrepancy is uncertain.

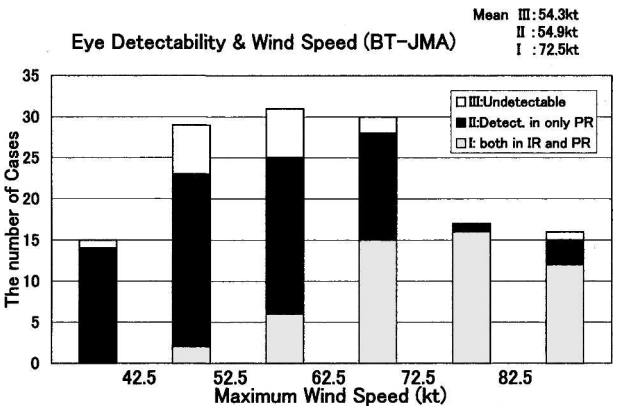

FIG. 4. Histogram of cases categorized by eye detectability in PR observations against the maximum 10-min sustained wind speed from BT-JMA data. Mean maximum wind speed averaged for each category is shown in the upper right.

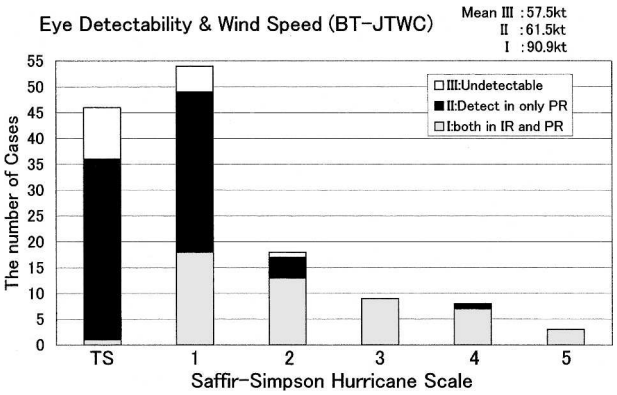

FIG. 5. As in Fig. 4, except against the maximum 1-min sustained wind speed from BT-JTWC data categorized by the Saffir–Simpson hurricane scale; TS: 34–63 kt, category 1: 64–82 kt, category 2: 83–95 kt, category 3: 96–113 kt, category 4: 114–135 kt, category 5: more than 135 kt. Mean maximum wind speed averaged for each category of eye detectability is shown in the upper right.

Figure 5 repeats Fig. 4, but uses maximum 1-min sustained winds from BT-JTWC. Classification of typhoon intensity was made following the Saffir–Simpson hurricane scale, including TSs, for which the maximum 1-min sustained wind is defined as between 34 and 64 kt. Most of the weaker storms, corresponding to TS or category 1 typhoons, and a part of category 2 typhoons, had detectable eyes only in the PR observations. This is consistent with the Dvorak technique, which does not classify systems without an eye in cloud images as typhoons, and can recognize typhoons as high as 102 kt without an eye detectable using the IR data (Dvorak 1984). In one case, a TS had a detectable eye in IR observations. This system was TS Sinlak at 0654 UTC on 30 August 2002, which developed rapidly, and the linear temporal interpolation of the 3- or 6-hourly wind speeds from BT-JTWC may have incorrectly estimated maximum wind speeds at the TRMM observation times. In one case, a category 2 typhoon had no detectable eye in the PR observations. This is the case shown in Fig. 3g when a trace of an eyewall was observed in the upper troposphere.

Eye detectability in PR and IR observations was examined for each life stage. Developing TCs had eyes in most cases in the PR data but not in the IR data (Table 3a). Most mature TCs had eyes in the PR data, but only about half had eyes in the IR data (Table 3b). Decaying TCs had eyes in the PR data in about 75% of cases, but an eye was detectable in only 31% of ring cases, a much smaller percentage than for other cases (Table 3c). Typhoon eyewalls frequently distorted during the decaying stage of the TC life cycle.

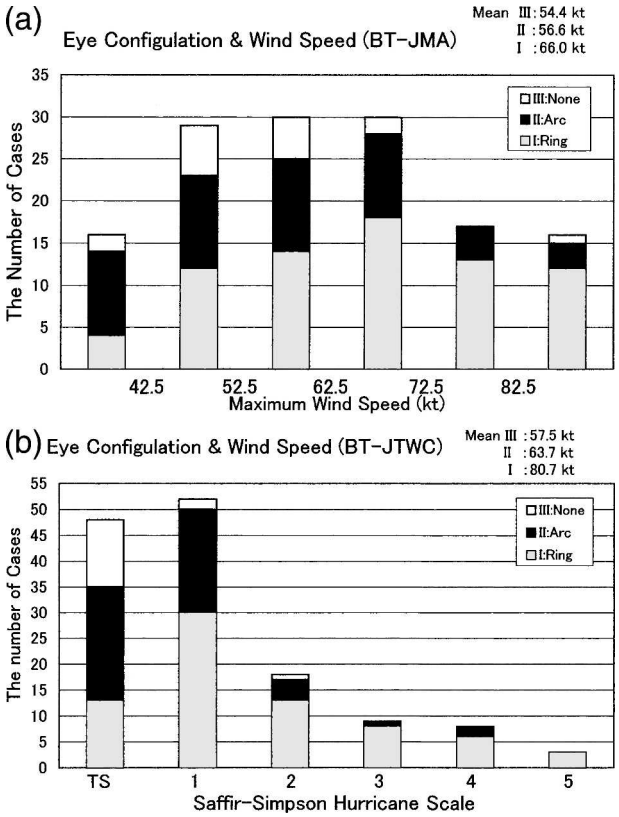

FIG. 6. (a) Histogram of the cases categorized with the eye configuration in PR observation against the maximum 10-min sustained wind speed from BT-JMA data. Mean wind speed for each category is shown in the upper right. (b) As in Fig. 6a except against the maximum 1-min sustained wind speed from BT-JTWC data. The maximum wind speed is categorized by the Saffir–Simpson hurricane scale as in Fig. 5.

5. Statistics of eye configuration

Precipitation radar observations reveal typhoon eyewall structures regardless of upper cloud cover. This study examines the statistical relationships between the eye configuration depicted in PR data, the TC life stage, and maximum sustained wind speeds (Table 4a). There was no strong relationship between the life stage and the number of ring and arc cases. However, concentric cases appeared most frequently in the mature stages. This finding is consistent with Willoughby et al. (1982), who showed the concentric eyewalls that sometimes appear in strong tropical cyclones and weaken them, and with Nakazawa et al. (2002), who found many cases of mature-stage TCs that were characterized by concentric eyewalls using 85-GHz TMI observations.

Another analysis related the cloud configuration determined in IR imagery with the TC life stage determined from a time sequence of central SLP (Table 4b). EYE cases were concentrated in the mature stage. Dominant categories differed between the developing and decaying stages. The ratio of CVB and EMB cases was even in the former, while CVB cases dominated in the latter. Table 5 shows the relationship between cloud configuration in IR data and eye configuration in PR data. For the EYE cases, ring cases were common. This means that a complete eyewall was frequently established when an eye was observed in IR images. For the EMB and CVB cases, arc and none cases become more common. Incomplete or no eyewalls were more likely when no eye was detected in IR images. However, a complete eyewall as categorized by ring appeared in more than a third of the cases when no eye was detected in the IR observations.

Figures 6a and 6b relate the eye configuration determined in PR observations to the maximum sustained wind speeds from BT-JMA and BT-JTWC data, respectively. Arc cases were confined to weaker TCs in both analyses. Ring cases appeared in every category of typhoon intensity; however, in both datasets the number of ring cases increased as the maximum sustained winds increased.

Figure 7 relates the eye diameter determined from PR observations to the life stage of TCs. Most TCs in the developing stage had eyes with diameters smaller than 62.5 km. In addition, many mature-stage TCs had eyes of that size. Eyes larger than 82.5 km in diameter were observed only in the mature and decaying stages,

TABLE 3a. As in Table 2, for the developing stage.

	Eye in IR	No eye in IR	Total
Ring in PR	7 (18%)	14 (35%)	21 (53%)
Arc in PR	0 (0%)	15 (38%)	15 (38%)
None in PR	0 (0%)	4 (10%)	4 (10%)
Total	7 (18%)	33 (83%)	40 (100%)

TABLE 3b. As in Table 2, but for the mature stage.

	Eye in IR	No eye in IR	Total
Ring in PR	27 (39%)	16 (23%)	43 (62%)
Arc in PR	8 (12%)	13 (19%)	21 (30%)
None in PR	0 (0%)	5 (7%)	5 (7%)
Total	35 (51%)	34 (49%)	69 (100%)

TABLE 3c. As in Table 2, but for the decaying stage.

	Eye in IR	No eye in IR	Total
Ring in PR	6 (21%)	3 (10%)	9 (31%)
Arc in PR	3 (10%)	10 (34%)	13 (45%)
None in PR	0 (0%)	7 (24%)	7 (24%)
Total	9 (31%)	20 (69%)	29 (100%)

TABLE 4a. The number of cases categorized by eye configuration in PR observations and life stage. The configuration is classified into ring, arc, none, and concentric, and life stages are classified into developing stage, mature stage, and decaying stage.

	Ring	Arc	None	Total	Concentric
Developing	21	15	4	40	4
Mature	43	21	5	69	11
Decaying	9	13	7	29	2

with one exception that was in the developing stage. Mean eye diameter increased for later life stages. Weatherford and Gray (1988) examined previous U.S. Air Force reconnaissance and concluded that in most typhoons, eyes as observed by airborne radar had diameters of less than 80 km (Fig. 17 of their paper). In their analysis, eyes with diameters exceeding 80 km were found in only 5% of the 138 cases in which typhoon eyes were detected. That percentage is smaller than the results in the present study, which found eyes exceeding 82.5 km in diameter in 19% of cases. The reason for this inconsistency, despite differences in the definition of eye size, is unclear.

The relationship between eye diameter determined from PR observations and cloud configuration as determined from Dvorak analysis of IR imagery is shown in Fig. 8. When IR imagery showed an EMB pattern, the eye diameter as determined by PR data was usually smaller than 62.5 km. If the PR data showed an eye with a diameter between 62.5 and 122.5 km, the EYE pattern was more common than other patterns. If the PR data showed a TC with a very large eye diameter (greater than 122.5 km), the CVB pattern was most common. Smaller eyes are more easily covered by upper-level cloud decks (EMB cases). Very large eyes are accompanied by distorted ring clouds and cannot be categorized as EYE in the Dvorak technique.

The relationship between eye diameters in the PR and IR observations was examined for cases when an eye was detected in both (Fig. 9). In most cases, the eye diameter was larger in the PR data. The upper-cloud shield reduces the size of the eye in IR images, as shown in Figs. 3c and 3d. Several cases, however, had a larger eye diameter in IR observations. These corresponded to TCs with concentric eyewalls, and the inner eyewall was shallow, as in Figs. 3i and 3j.

TABLE 4b. As in Table 4a, except that the eye configuration in IR observations is categorized by the Dvorak technique (EYE: eye detectable; CVB: curved band; EMB: embedded eye pattern; SHR: shear pattern).

	EYE	CVB	EMB	SHR	Total
Developing	8	14	15	3	40
Mature	34	18	13	4	69
Decaying	9	14	4	2	29

TABLE 5. The number of cases categorized by eye configuration in PR observations (ring, arc, none, and concentric) and cloud configuration in IR observations categorized by the Dvorak technique (EYE: eye detectable; CVB: curved band; EMB: embedded eye pattern; SHR: shear pattern).

	EYE	CVB	EMB	SHR
Ring	40	17	14	2
Arc	11	20	14	4
None	0	9	5	2
Total	51	46	33	8
Concentric	12	4	2	0

Figure 10 shows the relationship between eye diameter and the maximum 1-min sustained wind speed recorded in the BT-JWTC data. The cases when diameter of TC eyes exceeded 122.5 km as determined from PR data have been excluded from this analysis, because of the small number of the cases. The dominant eye diameter was less than 40 km when the maximum wind speed exceeded 110 kt or was less than 50 kt. This relationship is consistent with the analysis of airborne radar observations of typhoons by Weatherford and Gray (1988), which showed that dominant eye diameter was less than 40 km when minimum SLP was higher than 980 hPa or lower than 940 hPa (Fig. 15 of their paper), despite differences in the definition of a detectable eye and eye diameter in radar observations. Figure 10 also shows results for each life stage. In the developing stage, eye diameter decreased as the maximum wind speed increased. In the mature and decaying stages, eye diameter increased (decreased) as the maximum wind speed increased, when the wind speed was less (more) than 80 kt. Further studies are required to

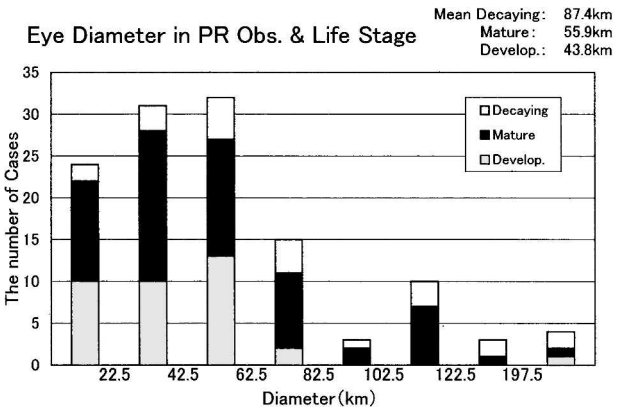

FIG. 7. Histogram of the cases categorized by life stage against the eye diameter measured in PR observations. Mean diameter averaged for each category is shown in the upper right.

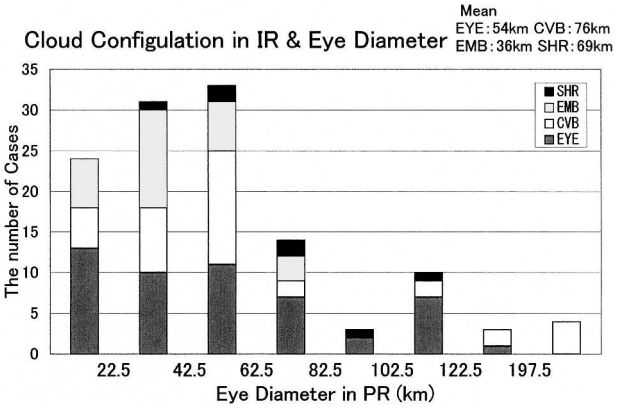

FIG. 8. Histogram of the cases categorized by cloud configuration in IR observations following the Dvorak technique against the diameter of TC eyes measured in PR observations. Mean diameter averaged for each category is shown in the upper right.

determine the statistical significance of these results and to clarify the mechanisms of them.

6. Summary and conclusions

This study examined the detectability of typhoon eyes in IR and PR observations from TRMM for 138 cases comprised of 61 TCs between 1998 and 2002. Tropical cyclone eyes were not detected in IR data in more than two-thirds of the cases. Eyes were detected in PR data in 89% of the cases. TCs without eyes in the PR data occurred most frequently in the decaying stage. Eye detectablity in the IR data was lower in the developing and decaying stages. Upper cloud shields

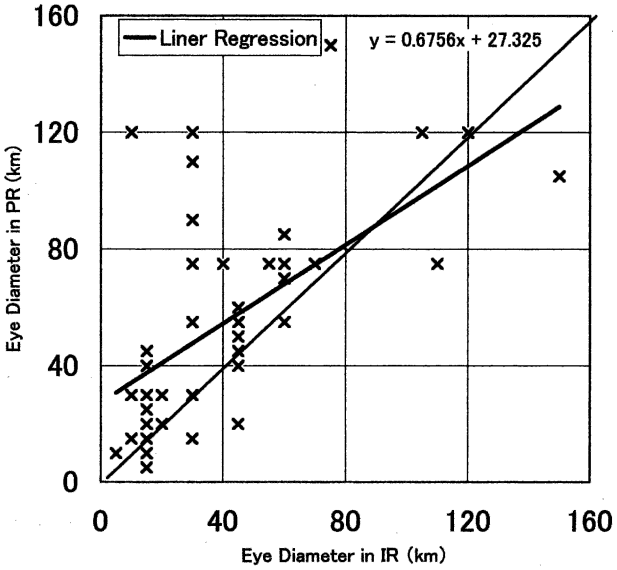

FIG. 9. Relationship of the diameter of TC eyes measured in PR and IR observations.

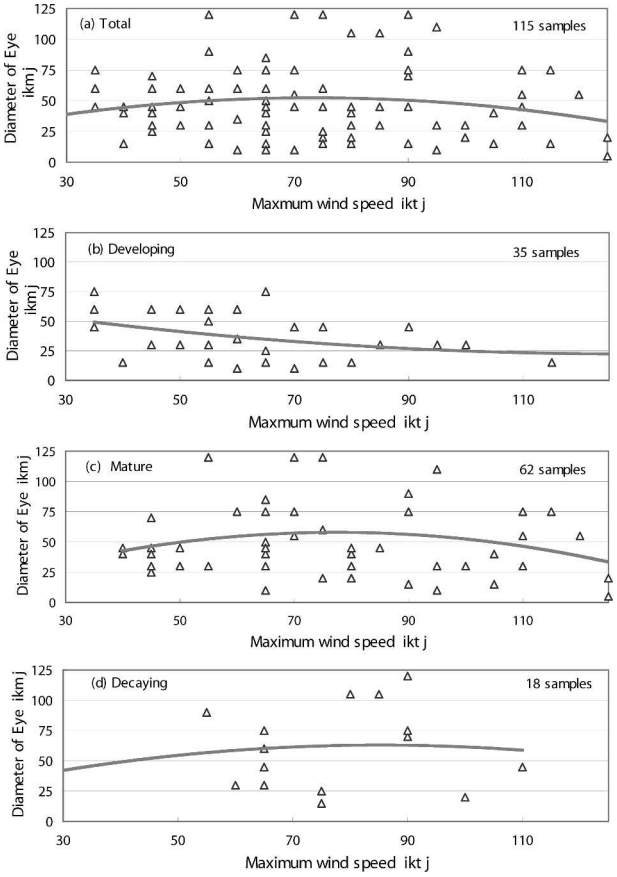

FIG. 10. Relationship between the eye diameter determined in PR and the maximum 1-min sustained wind speed from BT-JWTC data. (a) TCs with eyes exceeding 122.5 km in diameter were excluded. (b)–(d) As in (a) but for TCs in the (b) developing stage, (c) mature stage, and (d) decaying stage.

that obscured the TC eye were the main hindrance to eye observation in the IR data in the developing and mature stages. Concentric eyewalls appeared more frequently during the mature and decaying stages, a finding that is consistent with Willoughby et al. (1982). Eye diameter determined from PR observations increased for the later stages. Most TCs in the developing stage had eyes with diameters smaller than 62.5 km. In most cases, eye diameter was smaller in IR observations than in PR observations because the upper cloud shield can intrude over the precipitation free inner core. However, the eye diameter was smaller in the PR observations for several TCs with concentric rings. In such cases, the shallow inner eyewall appeared in the PR data, and the deep outer eyewall appeared in both the IR and PR data.

The Dvorak technique uses EMB or CVB methods to determine intensity when an eyewall is beginning to develop. Satellite cloud images often fail to provide the

analyst with an accurate low-level circulation center to assist with intensity determination. Precipitation radar observations can detect eyewalls in most TCs even in the developing stage. Precipitation radar observations thus have merit for practical application. Microwave observations at 85 GHz can also detect eyewalls (e.g., Cecil and Zipser 1999). The 85-GHz TBB highlights ice meteors in upper-tropospheric clouds, whereas PR observations yield the vertical cloud structure throughout the troposphere. Detailed examination of the merits and shortcomings of practical applications of PR and 85-GHz microwave observations are left to future studies.

Acknowledgments. TRMM 2A25 and 1B01 products were provided by NASA and JAXA. Best track data were provided by JMA and JTWC. QuikScat data were provided by Remote Sensing Systems under the sponsorship of NASA's Earth Science Enterprise (ESE). "TRMM Tropical Cyclones Database (version 1.1)" was produced by EORC, JAXA. This study was partly supported by a Grant-in-aid for Scientific Research (B) (Chief Scientist is Prof. K. Nakamura, Nagoya University) by JSPS and by a cooperative study between JAXA and Hirosaki University. The authors are grateful to comments from two anonymous reviewers that improved the original manuscript. We were also grateful to Mr. Akashi, JMA, for advice to the first author on how to apply the Dvorak technique to IR cloud images, to Prof. Ebuchi for comments on the QuikScat data, to Mr. Hirai, Ms. Kitabatake, and Drs. Yamagishi and Kurihara, for fruitful discussions on the relationship between 1- and 10-min sustained maximum wind speeds, and to Mr. Mannoji, Mr. Inaba, and Dr. Nagata for discussions regarding the classification of TCs by JMA. TRMM images were drawn using GrADS.

REFERENCES

Black, M. L., and H. E. Willoughby, 1992: The concentric eye wall cycle of Hurricane Gilbert. *Mon. Wea. Rev.,* **120,** 947–957.

Cecil, D. J., and E. J. Zipser, 1999: Relationship between tropical cyclone intensity and satellite-based indicators of inner core convection: 85-GHz ice-scattering signature and lightning. *Mon. Wea. Rev.,* **127,** 103–123.

Dvorak, V. F., 1975: Tropical cyclone intensity analysis and forecasting from satellite imagery. *Mon. Wea. Rev.,* **103,** 420–430.

——, 1984: Tropical cyclone intensity analysis using satellite data. NOAA Tech. Rep. NESDIS 11, 47 pp.

Koba, H., T. Hagiwara, S. Osano, and S. Akashi, 1990: Relationship between CI number from Dvorak's technique and the minimum sea level pressure or the maximum wind speed of tropical cyclones. *J. Meteor. Res.,* **42,** 59–67.

Lander, M. A., 1999: A tropical cyclone with a very large eye. *Mon. Wea. Rev.,* **127,** 137–142.

Mori, K., S. Ishigaki, T. Maehira, M. Ohya, and H. Takeuchi, 1999: Structure and evolution of convection within typhoon Yancy (T9313) in the early developing stage observed by the Keifu Maru radar. *J. Meteor. Soc. Japan,* **77,** 459–482.

Muramatsu, T., 1983: Diurnal variations of satellite measured Tbb areal distribution and eye diameter of mature typhoons. *J. Meteor. Soc. Japan,* **61,** 77–90.

Nakazawa, T., K. Besso, and S. Hoshino, 2002: A tropical cyclone intensity estimation technique from TRMM and other satellite data. *Extended Abstracts, First TRMM Int. Science Conf.,* Honolulu, HI, NASA and NASDA, 174.

NASA GSFC, 2002a: File specifications for TRMM products—Level 1. Tropical Rainfall Measuring Mission Science Data Information System: Interface Control Specification between the Tropical Rainfall Measuring Mission Science Data and Information System (TSDIS) and the TISDIS Science User (TSU), TISDIS-P907, Release 5.10, Vol. 3, 5_4–5_10.

——, 2002b: File specifications for TRMM products—Level 2 and 3. Tropical Rainfall Measuring Mission Science Data Information System: Interface Control Specification between the Tropical Rainfall Measuring Mission Science Data and Information System (TSDIS) and the TISDIS Science User (TSU), TISDIS-P907, Release 5.10, Vol. 4, 1_5–1_24.

Weatherford, C. L., and W. M. Gray, 1988: Typhoon structure as revealed by aircraft reconnaissance. Part II: Structural variability. *Mon. Wea. Rev.,* **116,** 1044–1056.

Willoughby, H. E., 1990: Temporal changes of the primary circulation in tropical cyclones. *J. Atmos. Sci.,* **47,** 242–264.

——, J. A. Clos, and M. G. Shoreibah, 1982: Concentric eye walls, secondary wind maxima, and the evolution of the hurricane vortex. *J. Atmos. Sci.,* **39,** 395–411.